# Topology of the phonon dispersion in $\alpha$-cristobalite

**Björn Wehinger[1], Alexeï Bosak[2], Keith Refson[3], Alessandro Mirone[2], Aleksandr Chumakov[2] and Michael Krisch[2]**

[1] Department of Quantum Matter Physics, University of Geneva, 24, Quai Ernest Ansermet, CH-1211 Genève, Switzerland

[2] ESRF - The European Synchrotron, 71, Avenue des Martyrs, F-38000 Grenoble, France, France

[3] STFC Rutherford Appleton Laboratory, Harwell Science and Innovation Campus, Oxfordshire OX11 0QX, United Kingdom

E-mail: `bjorn.wehinger@unige.ch`

**Abstract.** The lattice dynamics of the silica polymorph $\alpha$-cristobalite has been investigated by a combination of diffuse and inelastic x-ray scattering and *ab initio* lattice dynamics calculations. Phonon dispersion relations and vibrational density of states are reported and the phonon eigenvectors analysed by an intensive comparison of scattering intensities. The experimentally validated calculation is used to identify the vibration contributing most to the first peak in the density of vibrational states. The comparison of the displacement pattern to the silica polymorphs $\alpha$-quartz and coesite reveals a distinct similarity and allows for decisive conclusions on the vibrations causing the so-called Boson peak in silica glass on a local scale.

Submitted to: *New J. Phys.*

**Contents**



## 1. Introduction

Cristobalite, $SiO_2$, crystallises at high temperature to a cubic structure ($\beta$-phase) and undergoes a phase transition to its $\alpha$-phase upon cooling. $\alpha$-cristobalite has space group $P4_12_12$ and is stable at room temperature and ambient pressure [1]. Natural crystals are usually twinned [2]. The lattice dynamics of $\alpha$-cristobalite has attracted considerable interest due to its auxetic behaviour at molecular level [3–5] and the eventual realisation of a true surface wave occurring at a single isolated point within a bulk band [6]. It furthermore exhibits of a mass density (2.289(1) g/cm$^3$) very comparable to ambient silica glass (2.20(1) g/cm$^3$) and very similar thermodynamics properties [7]. It could in fact be shown, that the excess states over the Debye law in the vibrational density of states (VDOS) in absolute numbers are very similar for ambient silica glasses and ambient silica glass. The same is true for $\alpha$-quartz and densified silica glass with matched densities. These excess states, which give rise to the so called 'Boson peak' in glassy systems, are located at the same energies and provide the same heat capacity as in the crystals with matched densities. These observations strongly suggest that, similar to crystals, the excess of vibrational states in glasses originates from the piling up of the acoustic-like branches near the boundary of the pseudo-Brillouin zone. The experimental information on the lattice dynamics is limited to phonon frequencies at the Γ-point, elastic constants and thermodynamics properties [8–11]. A theoretical investigation of the phonon dispersion relation was performed using a Born-von-Karman force model [12], while calculations from first principles are again limited to the Γ-point [13].

In the following we use a combination of thermal diffuse scattering (TDS) and inelastic x-ray scattering (IXS) together with *ab initio* lattice dynamics calculations to study the full lattice dynamics of $\alpha$-cristobalite. The experimentally validated calculation is used to investigate the topology of the phonon dispersion in order to localize and identify the vibration contributing most to the first peak in the VDOS.

## 2. Experimental Details

Natural α-cristobalite crystals from the Ellora Caves, Hyderabad, India used in this study were kindly made available from the Harvard Mineralogical Museum collection. An octahedral single crystal with 0.2 mm along the four-fold axis was used for both thermal and inelastic x-ray scattering studies, which were conducted at room temperature. One major twin and some mosaic spread were observed during the x-ray diffuse scattering. One domain could be used for experimental study with very little contribution of the others. A synthetic polycrystalline sample (Materials Research Institute and School of Physics and Astronomy, Queen Mary University of London, UK) was used for the powder IXS measurements. The purity of the polycrystalline sample was verified by high-resolution x-ray diffraction at ID28. The samples revealed pure single-phase patterns. The crystalline quality was checked by x-ray diffuse scattering. Clear patterns of diffraction rings without noticeable effects of structural disorder were observed.

The x-ray diffuse scattering experiment was conducted on beamline ID29 [14] at the ESRF - The European Synchrotron. Monochromatic X-rays with wavelength 0.700 Å were scattered from the crystal in transmission geometry. The sample was rotated with an increment of 0.1° orthogonal to the beam direction over an angular range of 360° while diffuse scattering patterns were recorded in shutterless mode with a PILATUS 6M detector [15]. The orientation matrix and geometry of the experiment were refined using the CrysAlis software package. 2D reconstructions were prepared using locally developed software.

The single crystal IXS study was carried out on beamline ID28 at the ESRF. The spectrometer was operated at 17.794 keV incident energy, providing an energy resolution of 3.0 meV full-width-half-maximum and a horizontal momentum resolution of 0.3 $nm^{-1}$. Energy transfer scans were performed at constant momentum transfer (Q) in transmission geometry along selected directions in reciprocal space. Further details of the experimental setup and the data treatment can be found elsewhere [16].

The powder IXS study was conducted at ID28, too. IXS spectra were taken at momentum transfers chosen away from the Debye-Scherrer rings. The Q-range covered 10 to 70 $nm^{-1}$. The data combine measurements with 1.4 meV resolution at 23.725 keV incident energy within -25 to 25 meV and 0.2 meV energy steps and measurement with 3.0 meV resolution within -25 to180 meV and 0.7 meV steps. The elastic peak in the IXS spectra was subtracted using the instrumental resolution function determined from a polymethylmethacrylate (PMMA) sample close to the maximum of its structure factor. The generalised x-ray weighted VDOS (X-VDOS) was obtained by summing IXS spectra within the incoherent approximation following a previously described data treatment procedure [17].

## 3. Calculation

The lattice dynamics calculations were performed using density functional perturbation theory (DFPT) [18] as implemented in the CASTEP code [19, 20]. Local density approximation within the plane-wave formalism was employed using norm-conserving pseudopotentials of the optimized form [21]. Three reference orbitals were treated as valence states for Silicon and two for Oxygen. The plane wave cut-off and the sampling of the electronic grid were carefully tested by evaluating the convergence of internal forces. The electronic structure was computed on a $6 \times 6 \times 6$ Monkhorst-Pack grind and the plane wave cut-off was set to 800 eV. The cell geometry was optimized employing the Broyden-Fletcher-Goldfarb-Shannon method [22] by varying lattice and internal parameters. For the cell parameters of the optimised cell we find a = b = 4.939 Å and c = 6.870 Å. These values compare within 1.1% to those determined by x-ray diffraction (a = b = 4.97(8) Å and c = 6.94(8) Å [2]). Phonon frequencies and eigenvectors were computed on a $7 \times 7 \times 7$ Monkhorst-Pack grid of the irreducible part of the Brillouin zone by a perturbation calculation. Sum rules for the acoustic branches as well as the charge neutrality at the level of Born effective charges were imposed with a maximum correction of 1.2 meV at Γ. A Fourier interpolation with a grid spacing of 0.005 $Å^{-1}$ in the cumulant scheme including all image force constants was applied for the VDOS [23, 24]. The calculation was tested to be well converged with a maximum error in phonon energies of $< 0.05$ meV. Scattering intensities were calculated in first order approximation assuming the validity of both harmonic and adiabatic approximation [16].

## 4. Results

High symmetry reciprocal space sections of experimental diffuse scattering and calculated TDS intensity distributions are shown in Figure 1. A complex distribution of diffuse scattering is noticeable. The diffuse scattering in the H0L plane is more intense for low momentum transfers in the <1 0 1> direction, in particular between ($\bar{2}$ 0 0) and (0 0 2). Its origin was proven by IXS to be of elastic nature and corresponds to the inter-twin boundary. In the HHL plane we note streak like diffuse features along <1 1 0>, in agreement with the prediction of the rigid unit modes model [25] and the observation by electron diffraction [26]. Even stronger streaks are observed along <1 1 2>.

The streaks along <1 1 0> and <1 1 2> and some more directions were explored by IXS. A few prototypical scans are shown in Figure 2 and compared to calculated spectra. Some more IXS scans are summarised in the intensity maps along certain directions in Figure 3. The spectra are very well reproduced by the calculation. Applying a uniform scaling factor of 1.039 to the calculated phonon energies both energies and intensity of the phonon excitations match. The scaling factor was determined from the X-VDOS, and its value is justified further below. The overall agreement of experiment and calculation is very good. The minima of the lowest energy phonon branch are

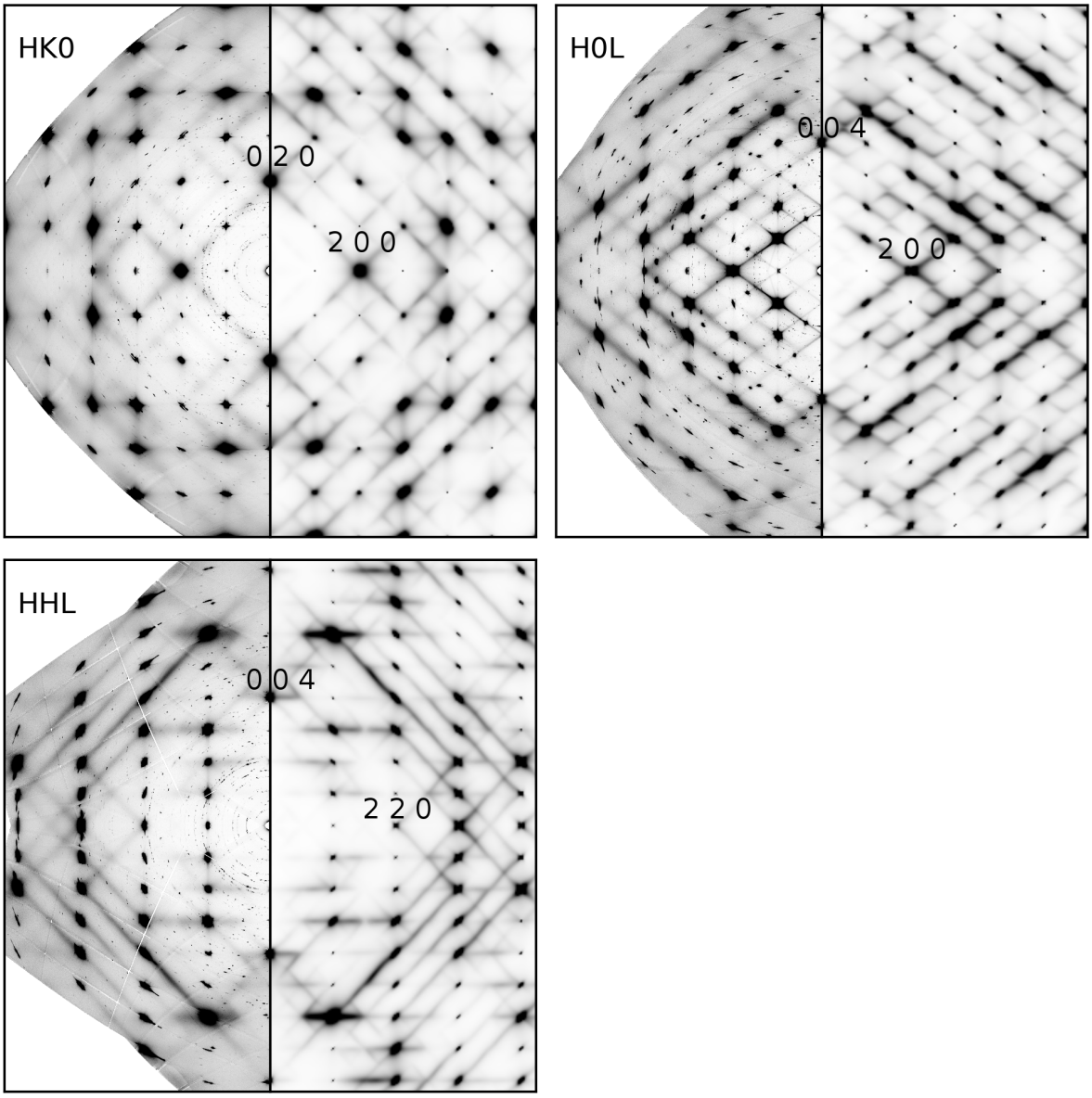


**Figure 1.** Experimental diffuse scattering (left part of individual panels) and calculated (right part of individual panels) TDS intensity distribution of single crystal α-cristobalite in the indicated reciprocal space sections. The experimental intensity distributions show signatures of the mosaic spread. See text for further details.

slightly underestimated in the showcases. A small elastic line is also present in all spectra. Figure 2a) and b) shows the IXS intensity map along <1 1 0> and <1 1 2>, respectively. Remarkably, we note quite flat phonon branches with energies around 5 meV. The calculation underestimates the energies of these bands slightly.

Calculated dispersion relations along high symmetry directions together with experimental values from the IXS measurements are shown in Figure 4. The phonon energies at the Γ point are compared to infrared [10] and Raman measurements [8, 9] as well as to *ab initio* calculated values from [13]. We note good agreement of our

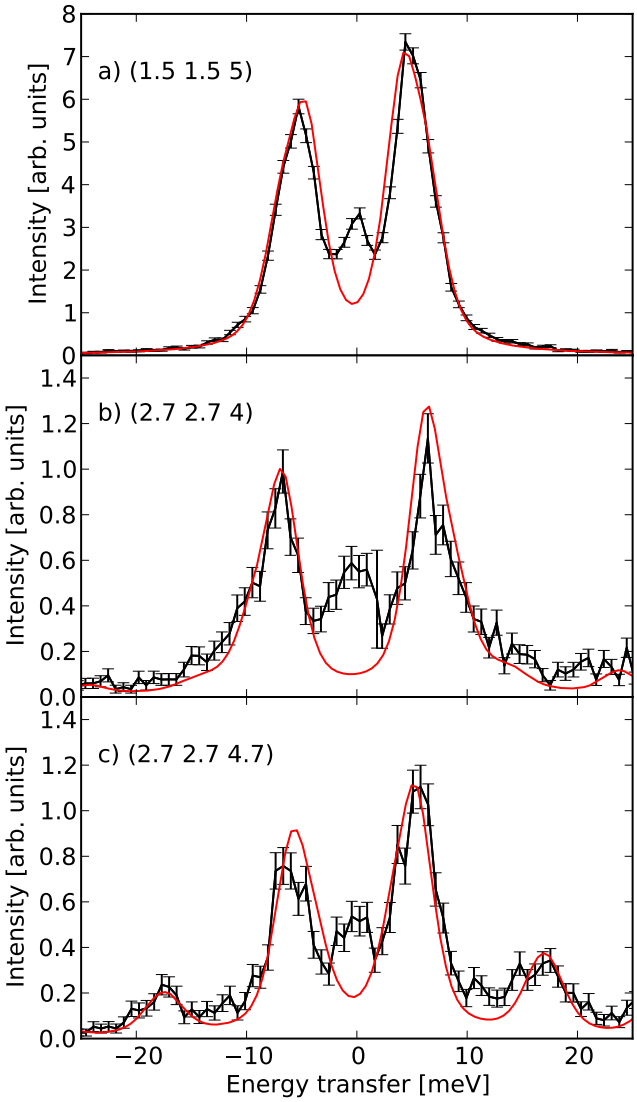


**Figure 2.** Experimental (black points with error bars) and theoretical (red line) IXS spectra of single crystal $\alpha$-cristobalite at the indicated reciprocal space points. Theoretical intensities were convoluted with the experimental resolution function and the energy transfer was scaled by 1.039. The excitation in the spectrum at M point (a) contains the contribution of two branches, see Figure 4.

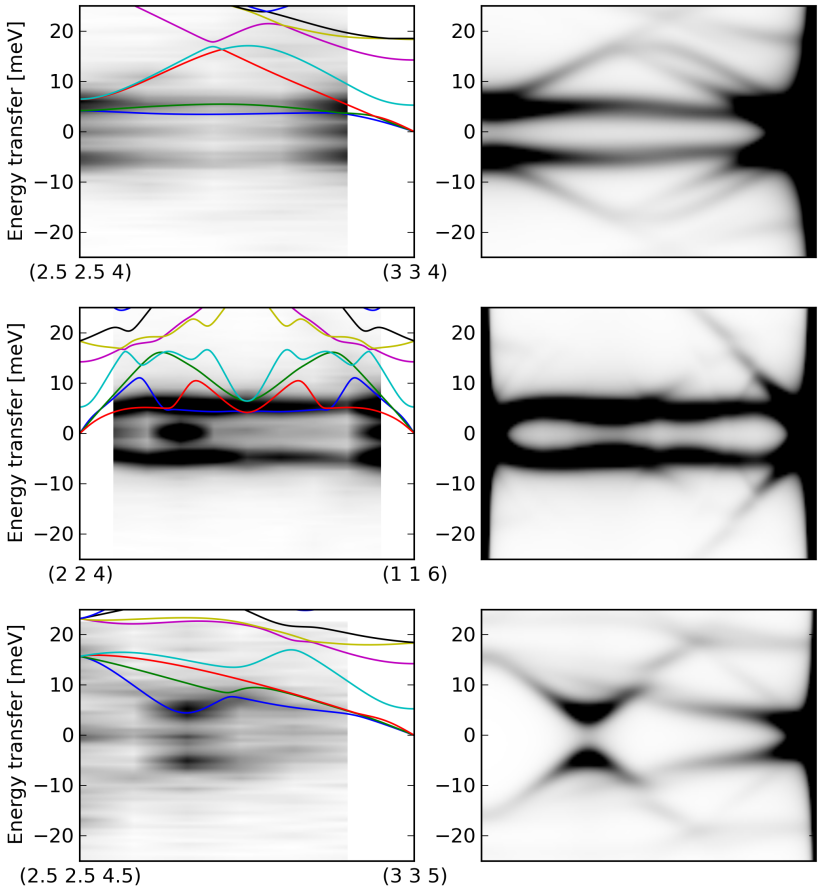


**Figure 3.** Experimental IXS intensity maps (left panels) from $\alpha$-cristobalite crystal together with theoretical intensity maps along the indicated directions (right panels). The experimental maps in a) consist of 5 and in b) and c) of 8 measured spectra with linear $\boldsymbol{q}$-spacing and energy steps of 0.7 meV. The momentum- and energy-transfers are linearly interpolated to 200 q-points and 72 energy steps. The theoretical dispersion relations are traced as lines. The theoretical maps were calculated from the eigenvectors and eigenfrequencies for 200 points along a given direction in reciprocal space and convoluted with the experimental resolution function of the spectrometer. The absolute intensity is scaled for best visualisation of the inelastic features.

calculation with all experimental values, whereas the calculated values from [13] are significantly different.

The X-VDOS for $\alpha$-cristobalite is shown in Figure 5 a) and the calculated real VDOS in Figure 5 d). A linear scaling of all calculated phonon energies by 1.039 leads to an almost perfect agreement of experimental and theoretical X-VDOS over the complete energy range. The applied scaling factor is very similar to what is found for the tetrahedral coordinated silica polymorphs $\alpha$-quartz, coesite and stishovite [27–

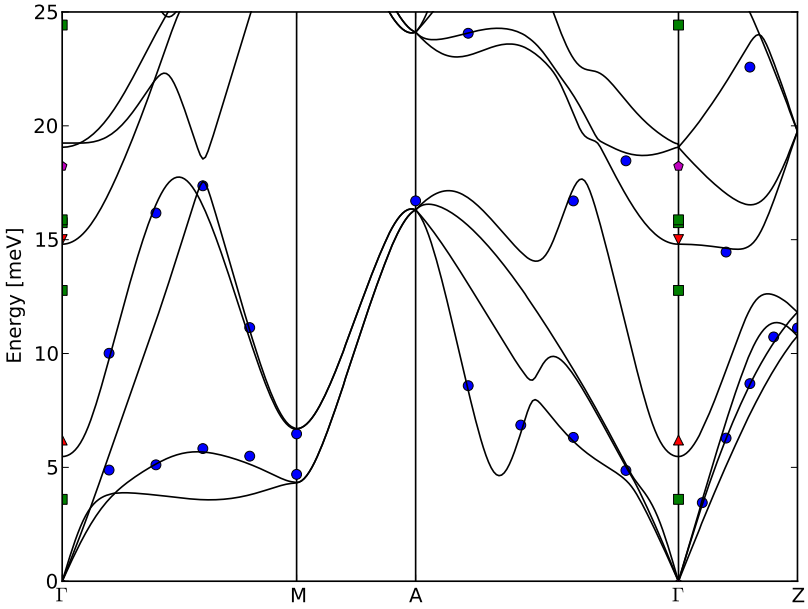


**Figure 4.** Phonon dispersion relations of α-cristobalite along high symmetry directions as obtained from the calculation (black lines) and the single crystal IXS experiment (blue points).The phonon energies at the Γ point are compared to Infrared [10] (magenta diamonds) and Raman measurements [8] (red triangles up) and [9] (red triangles down) as well as *ab initio* calculated values from [13] (green squares). The energies of our calculation are scaled by 1.039.

29]. We observe some very small discrepancies between experiment and theory, which are mainly due to the limited accuracy of sampling the reciprocal space with powder IXS spectra. The first peak in the VDOS is observed at a slightly higher energy as calculated (the discrepancy is 0.9 meV after the applied scaling). The partial density of states (Figure 5 b and c)) separate the contribution of silicon and oxygen atoms. Focusing on the low energy part of the partial VDOS (Figure 5 e)) we find that the first peak located at 4.56 meV is slightly dominated by the vibration of the oxygen atoms. The low energy VDOS of α-quartz is plotted in Figure 5 f) for comparison. We note that the first peak of the VDOS of α-cristobalite is located at significant lower energy than in α-quartz. In α-cristobalite the partial contribution of oxygen atoms is slightly higher than in α-quartz.

The localisation of critical points contributing most to the first peak of the VDOS was conducted by the simultaneous application of two filters. An energy filter of $\Delta E$= 0.3 meV was applied to the *ab initio* calculated phonon energies of the first Brillouin zone, and $1/|\nabla_{\boldsymbol{q}} E(\boldsymbol{q})|$ was computed within this energy window. The investigation reveals two saddle points with the same phonon energy contributing to the first peak in the VDOS of α-cristobalite. The computation of the local contribution within a cube in reciprocal space of $\Delta q = 1$ nm$^{-1}$ shows that the first peak arises mainly from the region

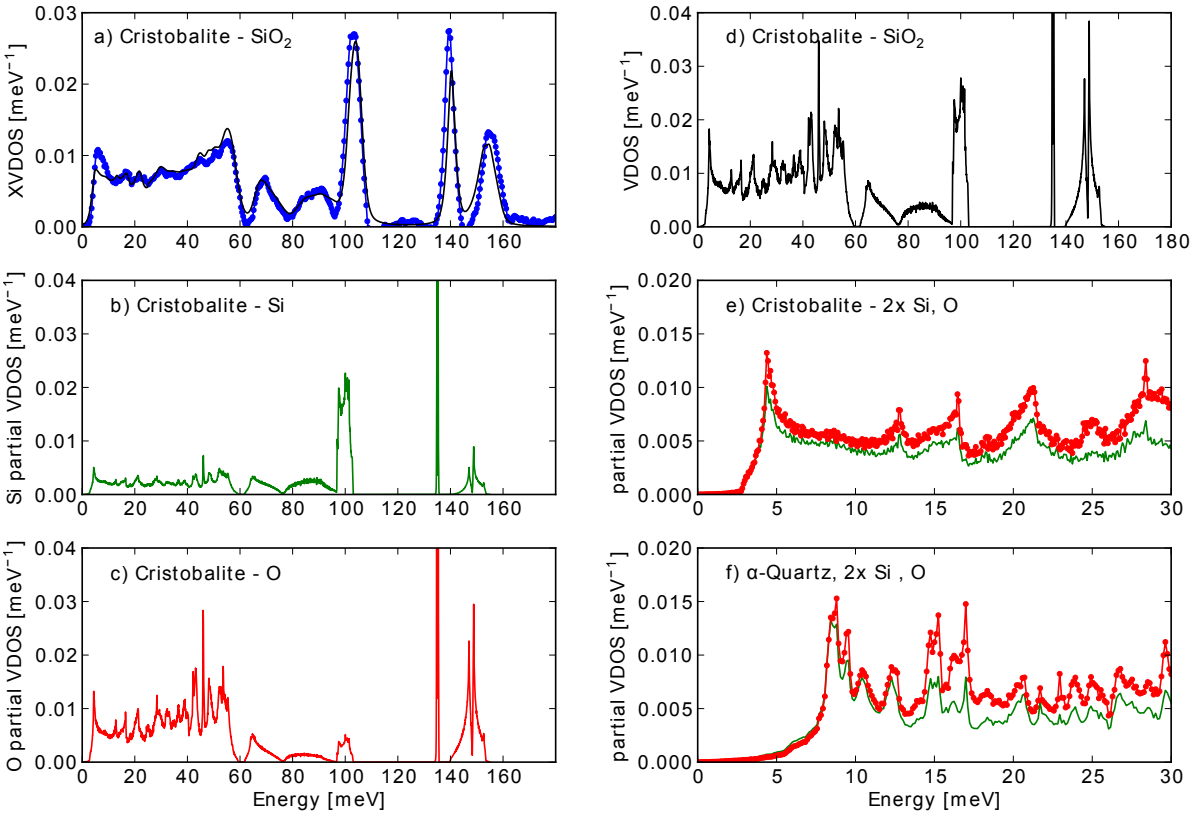


**Figure 5.** a) Experimental (blue points) and calculated (black line) X-VDOS of α-cristobalite. The calculated X-VDOS was convoluted with the experimental resolution function and the energies scaled by 1.039. The partial VDOS of oxygen and silicon and the VDOS are shown in b), c) and d), respectively. The partial VDOS of oxygen (red dots) and silicon (green line) of the low energy part are compared in (e), where the silicon contribution is multiplied by a factor of two. f) Partial VDOS of oxygen (red dots) and silicon (green line) in the low-energy range of α-quartz. The silicon contribution is multiplied by a factor of two.

around the M point (1/2 1/2 0). The local contribution is shown in Figure 6 a). The phonon dispersion surface containing the critical point shows a double degeneracy along <1 0 0>, <0 1 0> and <0 0 1>, which is split along the <1 1 0> direction, see Figure 6 b). The lower sheet forms a saddle point whereas the upper sheet forms a minimum which is of parabolic nature close to M. The peak in the VDOS arises thus from the lower branch for topological reasons [30]. The topology of the energy surface projected on the HK0 and HHL plane is shown in Figure 6 c) and d). A second saddle point with the same phonon energy located at (0.47 0.2 0.33) was found to have a smaller local contribution to the VDOS.

The VDOS and the displacement pattern contributing most to its first peak of α-cristobalite is compared in Figure 7 with the silica polymorphs α-quartz and coesite [28]. We note, that the low energy part of the VDOS is different. In particular the first peak in the VDOS is located at different energies. Quite remarkable is the fact that the critical points which are responsible for the first peak are located at the zone

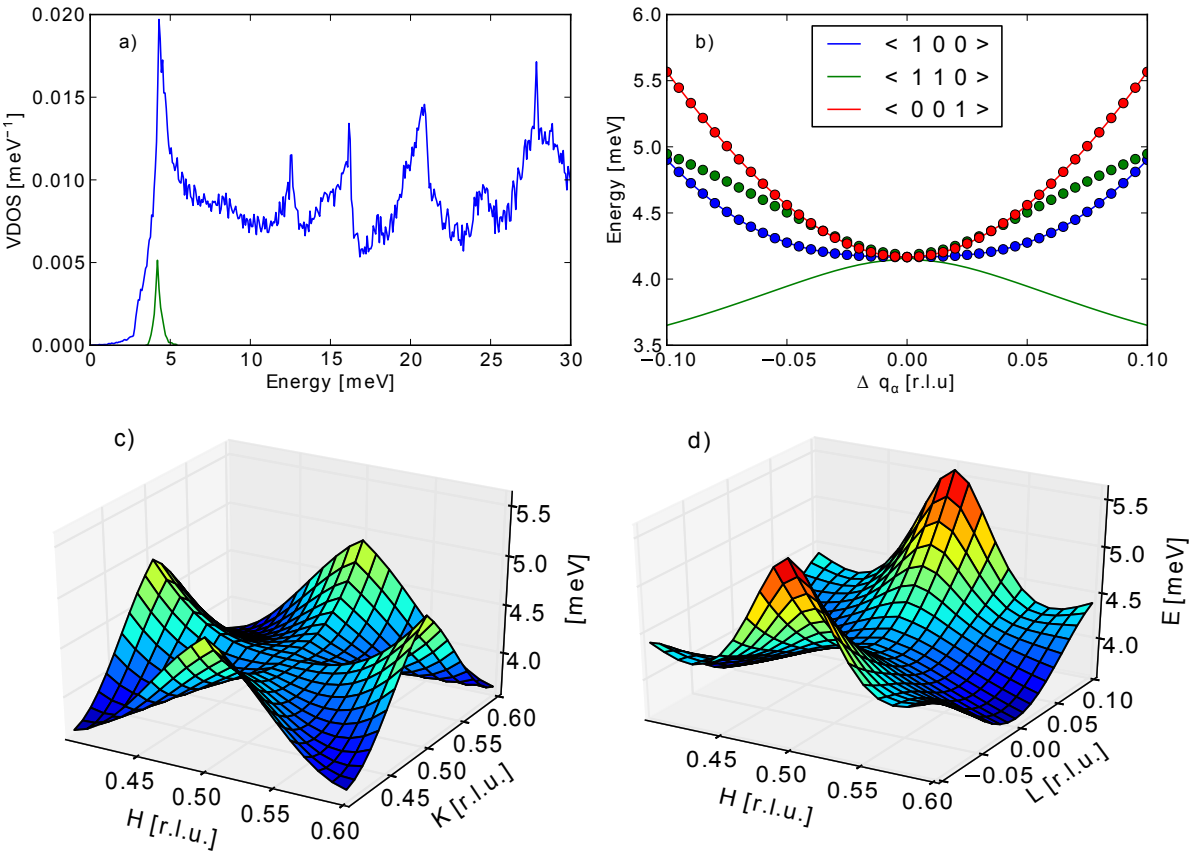


**Figure 6.** Contribution and topology of the critical point responsible for the first van Hove singularity in α-cristobalite. a) VDOS (blue) and the contribution of the energy surface containing the critical point at M (1/2 1/2 0) within $\Delta q = 1$ nm$^{-1}$ (green). b) Dispersion relations of the two branches containing the critical point along the indicated directions. The straight lines belong to the energy surface containing the saddle point; the dots belong to the sheet containing a minimum. c) and d) Energy surface projections of the dispersion surface containing the saddle point in the HK0 and HHL plane, respectively.

boundary in the case of all three silica polymorphs under investigation. The topology of the energy surface in the vicinity of the critical points is different, but despite this, the associated displacement patterns are very similar: The largest displacement is observed for oxygen. The vibration consists mainly of a tetrahedron tilt, accompanied by a small distortion.

## 5. Discussion and Summary

The VDOS, obtained from powder IXS spectra, probes the ensemble of vibrational states and was used to determine an overall scaling factor for the *ab initio* calculation. The application of a linear scaling factor of a few per cent leads to a very good agreement between *ab initio* calculated and measured phonon energies. The underestimation of the calculated energies can be attributed to the limited accuracy of the exchange correlation

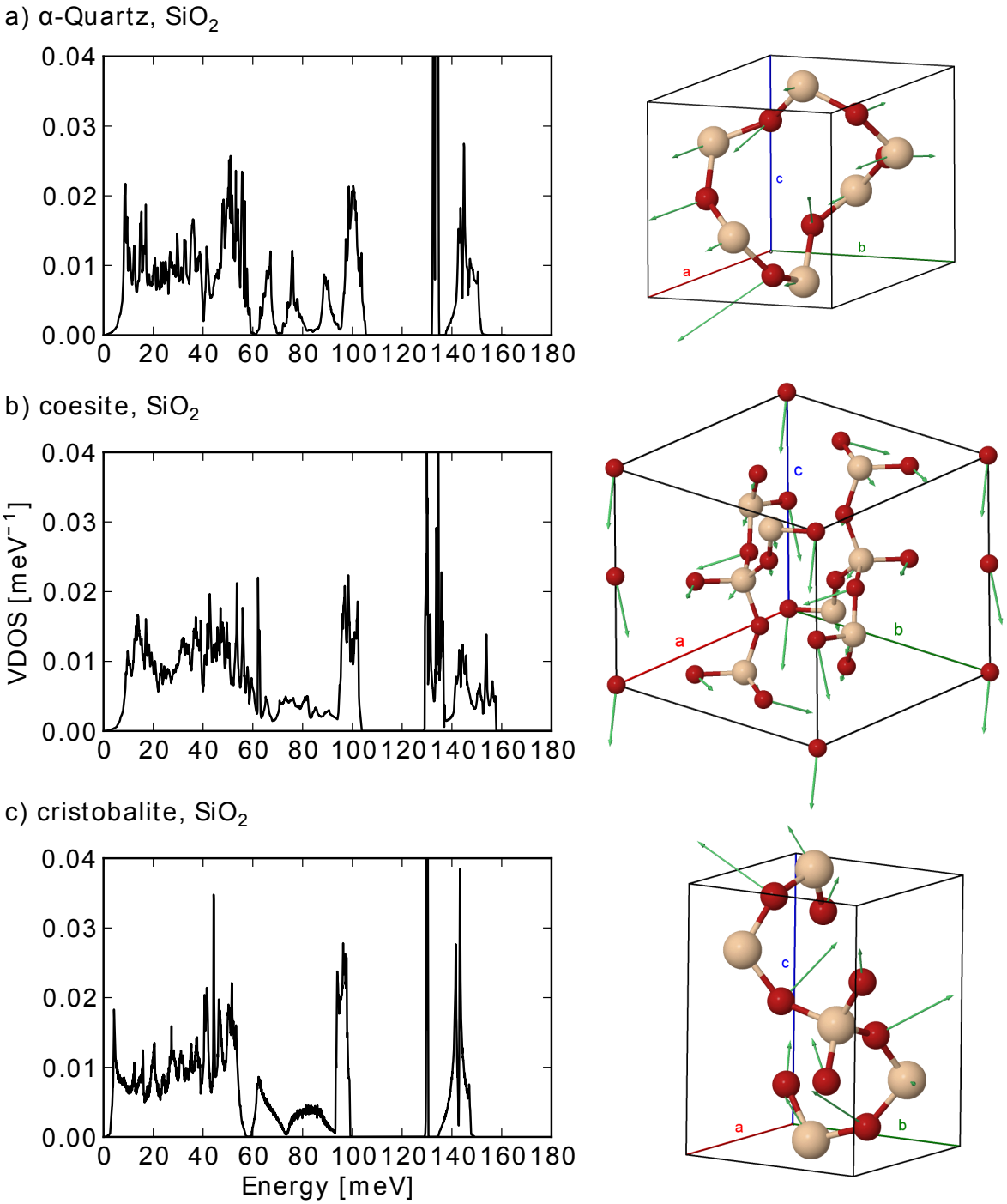


**Figure 7.** Calculated VDOS of $SiO_2$ $\alpha$-quartz (a), coesite (b) and $\alpha$-cristobalite (c). The displacement patterns of the vibrations contributing most to the first peak in the VDOS within the unit cell are illustrated on the right. Silicon atoms are marked beige, oxygen atoms red. Direction and amplitude of the eigenvectors are depicted in green arrows, in arbitrary scale for best visualisation.

function within the local density approximation and the fact that the calculation does not include any temperature effects, detailed discussions can be found elsewhere [20, 31].

By comparing TDS and IXS intensities over and extended region in reciprocal space, the calculation can be validated not only in terms of phonon energies but also in terms of phonon eigenvectors. The recovery of the complete lattice dynamics becomes possible. The full description of the lattice dynamics at arbitrary momentum transfer in turn allows for a topological investigation of the phonon dispersion. The critical points responsible for Van Hove singularities can be localized by the simultaneous application of an energy and gradient filter to the calculated phonon frequencies. The eigenvectors and the topology in energy-momentum space of the vibration contributing most to the first peak in the VDOS can be assigned and compared to the tetrahedrally coordinated silica polymorphs $\alpha$-quartz and coesite. Although the first peak in the VDOS is located at different energies and the topology of the energy surface in the vicinity of the critical points differs, a unifying picture on its origin can be drawn: The critical points are located at the zone boundary. The vibration contributing most to this first peak is mainly driven by oxygen vibration and consists of a tetrahedron tilt, accompanied by a small distortion. Comparing the VDOS of ambient silica glass and $\alpha$-cristobalite reveals that the number of excess states above the Debye levels are very similar (6.2(9) % and 6.8(9)%, respectively, [7]). For both systems, the first peak in the VDOS is located nearly at the same energy. The same is true for densified glass and $\alpha$-quartz, if the densities are matched. Taking into account the similarity observed in the displacement patterns of the investigated three silica polymorphs we can now conclude, that the vibration causing the Boson peak in silica glass must be similar as well on a local scale.

In summary we have seen, that the lattice dynamics of $\alpha$-cristobalite can be very well described by DFPT in the local density approximation. The thermal diffuse scattering shows a rich structure, including features, which were predicted by the theory of rigid unit modes. The single crystal IXS experiment allowed for a separation of elastic and inelastic contribution. A full description of phonon frequencies and eigenvectors could be retrieved and topological investigation of specific features in the lattice dynamics became possible.

In the framework of the silica polymorphs we are now able to provide accurate models of the lattice dynamics of $\alpha$-quartz, coesite, $\alpha$-cristobalite and stishovite [27–29]. The calculation for these polymorphs can be extended to high pressures and allow the derivation of thermodynamical properties. The prediction of the lattice dynamics for new high pressure phases like seifertite and others [32] should be possible within the employed calculation scheme.

## Acknowledgment

The authors would like to acknowledge the courtesy of the Harvard Mineralogical museum and personally the collection curator Dr. Raquel Alonso-Perez for providing the high quality pieces of natural cristobalite crystals (Cristobalite, HMM#97849) and

Martin Dove (Materials Research Institute and School of Physics and Astronomy, Queen Mary University of London, UK) for the polycrystalline sample.

## References

[1] J. J. Pluth, J. V. Smith, and J. Faber. Crystal structure of low cristobalite at 10, 293, and 473 K: Variation of framework geometry with temperature. *J. Appl. Phys.*, **57**, 1045–1049, (1985).

[2] W. A. Dollase. Reinvestigation of the structure of low cristobalite. *Z. Kristallogr.*, **121**(5), 369–377, (1965).

[3] A. Yeganeh-Haeri, D. J. Weidner, and J. B. Parise. Elasticity of α-cristobalite: A silicon dioxide with a negative poisson's ratio. *Science*, **257**(5070), 650–652, (1992).

[4] H. Kimizuka, H. Kaburaki, and Y. Kogure. Mechanism for negative poisson ratios over the α- β transition of cristobalite, $SiO_2$: A molecular-dynamics study. *Phys. Rev. Lett.*, **84**, 5548–5551, (2000).

[5] A. Alderson and K. E. Evans. Molecular origin of auxetic behavior in tetrahedral framework silicates. *Phys. Rev. Lett.*, **89**, 225503, (2002).

[6] D. Trzupek and P. Zieliński. Isolated true surface wave in a radiative band on a surface of a stressed auxetic. *Phys. Rev. Lett.*, **103**, 075504, (2009).

[7] A. I. Chumakov, G. Monaco, A. Fontana, A. Bosak, R. P. Hermann, D. Bessas, B. Wehinger, W. A. Crichton, M. Krisch, R. Rüffer, G. Baldi, G. Carini Jr., G. Carini, G. D'Angelo, E. Gilioli, G. Tripodo, M. Zanatta, B. Winkler, V. Milman, K. Refson, M. T. Dove, N. Dubrovinskaia, L. Dubrovinsky, R. Keding, and Y. Z. Yue. Role of disorder in the thermodynamics and atomic dynamics of glasses. *Phys. Rev. Lett.*, **112**, 025502, (2014).

[8] J. Bates. Raman spectra of α and β cristobalite. *J. Chem. Phys.*, **57**, 4042–4047, (1972).

[9] V. N. Sigaev, E. N. Smelyanskaya, V. G. Plotnichenko, V. V. Koltashev, A. A. Volkov, and P. Pernice. Low-frequency band at 50 $cm^{-1}$ in the Raman spectrum of cristobalite: identification of similar structural motifs in glasses and crystals of similar composition. *J. Non-Cryst. Solids*, **248**(2-3), 141 – 146, (1999).

[10] I. P. Swainson, M. T. Dove, and D. C. Palmer. Infrared and Raman spectroscopy studies of the $\alpha - \beta$ phase transition in cristobalite. *Phys. Chem. Miner.*, **30**(6), 353–365, (2003).

[11] W. Pabst and E. Gregorova. Elastic properties of silica polymorphs - a review. *Ceramics-Silikaty*, **57**(3), 167–184, (2013).

[12] G. Hua, T. Welberry, and R. Withers. Lattice dynamics of α- and β-cristobalite, $SiO_2$. *Journal of Physics and Chemistry of Solids*, **50**(2), 207 – 213, (1989).

[13] S. Coh and D. Vanderbilt. Structural stability and lattice dynamics of $SiO_2$ cristobalite. *Phys. Rev. B*, **78**, 054117, (2008).

[14] D. de Sanctis, A. Beteva, H. Caserotto, F. Dobias, J. Gabadinho, T. Giraud, A. Gobbo, M. Guijarro, M. Lentini, B. Lavault, T. Mairs, S. McSweeney, S. Petitdemange, V. Rey-Bakaikoa, J. Surr, P. Theveneau, G. Leonard, and C. Mueller-Dieckmann. ID29: a high-intensity highly automated ESRF beamline for macromolecular crystallography experiments exploiting anomalous scattering. *J. Synchrotron Radiat.*, **19**(3), 455–461, (2012).

[15] P. Kraft, A. Bergamaschi, C. Broennimann, R. Dinapoli, E. F. Eikenberry, B. Henrich, I. Johnson, A. Mozzanica, C. M. Schlepütz, P. R. Willmott, and B. Schmitt. Performance of single-photon-counting PILATUS detector modules. *J. Synchrotron Radiat.*, **16**(3), 368–375, (2009).

[16] M. Krisch and F. Sette. *Inelastic X-ray Scattering from Phonons. Light Scattering in solids, Novel Materials and Techniques, Topics in Applied Physics 108*. Springer-Verlag, (2007).

[17] A. Bosak and M. Krisch. Phonon density of states probed by inelastic x-ray scattering. *Phys. Rev. B*, **72**, 224305, (2005).

[18] X. Gonze and C. Lee. Dynamical matrices, born effective charges, dielectric permittivity tensors, and interatomic force constants from density-functional perturbation theory. *Phys. Rev. B*, **55**, 10355–10368, (1997).

[19] S. Clark, M. Segall, C. Pickard, P. Hasnip, M. Probert, K. Refson, and M. Payne. First principles methods using CASTEP. *Z. Kristallogr.*, **220**, 567–570, (2005).

[20] K. Refson, P. R. Tulip, and S. J. Clark. Variational density-functional perturbation theory for dielectrics and lattice dynamics. *Phys. Rev. B*, **73**, 155114, (2006).

[21] A. M. Rappe, K. M. Rabe, E. Kaxiras, and J. D. Joannopoulos. Optimized pseudopotentials. *Phys. Rev. B*, **41**, 1227–1230, (1990).

[22] B. G. Pfrommer, M. Côté, S. G. Louie, and M. L. Cohen. Relaxation of crystals with the quasi-newton method. *J. Comput. Phys.*, **131**(1), 233 – 240, (1997).

[23] X. Gonze, J.-C. Charlier, D. Allan, and M. Teter. Interatomic force constants from first principles: The case of α-quartz. *Phys. Rev. B*, **50**, 13035–13038, (1994).

[24] K. Parlinski, Z. Q. Li, and Y. Kawazoe. First-principles determination of the soft mode in cubic $ZrO_2$. *Phys. Rev. Lett.*, **78**, 4063–4066, (1997).

[25] M. T. Dove, A. K. A. Pryde, V. Heine, and K. D. Hammonds. Exotic distributions of rigid unit modes in the reciprocal spaces of framework aluminosilicates. *J. Phys.: Condens. Matter*, **19**(27), 275209, (2007).

[26] R. L. Withers, J. G. Thompson, and T. R. Welberry. The structure and microstructure of α-cristobalite and its relationship to β-cristobalite. *Phys. Chem. Minerals*, **16**(6), 517–523, (1989).

[27] A. Bosak, M. Krisch, D. Chernyshov, B. Winkler, V. Milman, K. Refson, and C. Schulze-Briese. New insights into the lattice dynamics of α-quartz. *Z. Kristallogr.*, **227**(2), 84–91, (2012).

[28] B. Wehinger, A. Bosak, A. Chumakov, A. Mirone, B. Winkler, L. Dubrovinsky, N. Dubrovinskaia, V. Brazhkin, T. Dyuzheva, and M. Krisch. Lattice dynamics of coesite. *Journal of Physics: Condensed Matter*, **25**(27), 275401, (2013).

[29] A. Bosak, I. Fischer, M. Krisch, V. Brazhkin, T. Dyuzheva, B. Winkler, D. Wilson, D. Weidner, K. Refson, and V. Milman. Lattice dynamics of stishovite from powder inelastic x-ray scattering. *Geophys. Res. Lett.*, **36**(19), (2009).

[30] L. Van Hove. The occurrence of singularities in the elastic frequency distribution of a crystal. *Phys. Rev.*, **89**, 1189–1193, (1953).

[31] L. He, F. Liu, G. Hautier, M. J. T. Oliveira, M. A. L. Marques, F. D. Vila, J. J. Rehr, G.-M. Rignanese, and A. Zhou. Accuracy of generalized gradient approximation functionals for density-functional perturbation theory calculations. *Phys. Rev. B*, **89**, 064305, (2014).

[32] L. S. Dubrovinsky, N. A. Dubrovinskaia, V. Prakapenka, F. Seifert, F. Langenhorst, V. Dmitriev, H. P. Weber, and T. Le Bihan. A class of new high-pressure silica polymorphs. *Phys. Earth Planet. Inter.*, **143–144**(0), 231 – 240, (2004).